Supplemental Information

Supplemental Materials and Methods

Phagocytosis assays

Phagocytosis assays were performed essentially as described [1]. using LabTek 8-well chamber slides (surface area approximately 0.8 cm², maximum volume 400 µL) (Ref. 177402PK. Thermo Fisher) at a multiplicity of infection (MOI) of 10. The cell line used was IC-21 (ATCC TIB-186) murine peritoneal macrophages. Macrophages (5 or 7×10^5 cells/well) were seeded 24 to 48 hours before infection. After 24 hours, cells were checked for proper adherence and morphology; if the cells were well adherent, the phagocytosis experiment was initiated, otherwise incubation was extended for an additional 24 hours. Cells were maintained below confluence prior to infection. From conidia stock suspension stored at 4°C, the required number of FITC-stained conidia per well was prepared in 100 µL of complete culture medium (RPMI supplemented with 10% fetal bovine serum and 1% penicillin-streptomycin) (Ref. 11504566. Fischer Scientific) to achieve an MOI of 10. For infection, the medium was removed from cells, and 100 µL of medium containing conidia was added to each well to reach the desired MOI. Phagocytosis was synchronized by placing the infected cells at 4°C for 30 minutes, followed by removal of the medium to eliminate non-adherent spores. Subsequently, 150 µL of complete culture medium was added, and the cells were incubated at 37°C and analyzed after the indicated incubation time.

Growth rates/colony expansion rate of *Afm* strains

Growth rates were evaluated on agar plates (indicated media) as follows. Conidia (10^6) were point-inoculated and plates incubated at 37 °C in the dark. At 18, 24, 48 and 60 hours, colony diameters were measured, and colonies expansion rates calculated from linear slopes of growth curves. Expansion rate was used as a proxy of growth rate.

Osmotic stress

Afm conidia (10^6) were point-inoculated on MM medium with glucose supplemented with 0.6 M NaCl or KCl and incubated at 37 °C in the dark. Colonies were imaged at 24, 48 and 72 h. Conidia yields were measured by gently washing plate with 5 mL of sterile milliQ water containing 0.1 % Tween-20, then filtered through a 40 µm cell strainer (ref. 0999225, Grosseron). The concentration of conidia in each sample was determined using a LUNA-FL cell counter (ref.59506, Dutscher).

Regulation of Erg-Asp synthesis in response to nitrogen depletion

Experiments showing that Erg-Asp decreases under nitrogen deprivation were conducted as follows: conidia were diluted to 10^6 conidia/mL in 50 mL MMG (MM with glucose) liquid medium and grown 18 h (overnight) at 37 °C under shaking (220 rpm) until mycelium pellets developed. Mycelia were then collected by pouring the culture onto a two-layer gauze filter, extensively washed on gauze with sterile H_2O, and then washed with sterile MMG or MMX before being resuspended in 50 mL liquid MMG or MMX, respectively. Mycelia were further

grown for 5 h at 37 °C under shaking (220 rpm). Mycelia were then collected as described, washed and frozen at -20 °C until use or directly processed for lipid extraction.

1. Mech, F., Thywißen, A., Guthke, R., Brakhage, A. A. & Figge, M. T. Automated Image Analysis of the Host-Pathogen Interaction between Phagocytes and Aspergillus fumigatus. *PLoS One* **6**, e19591 (2011).

Legends to supplemental Figures

Supplemental Fig. S1| Construction and phenotyping of *Afm* and *Mor* mutant strains. A. *Top panel.* TLC of total lipids extracted from indicated *Afm* strains grown under repressing (2 % Glc) or inducing (2 % Xyl) conditions, visualized under natural (top) or UV light (bottom). A control lane of total lipids from an *Sce* strain expressing *Afm* ErdS was used (*Sce* + ErdS). *Bottom panel.* WT, Δ*erdS* and Δ*erdS*::P_{Xyl}-*erdS* strains were grown in liquid cultures in the presence of the indicated amounts of Glc (repressor) and/or Xyl (inducer) to verify that increasing concentrations of Xyl triggered overproduction of Erg-Asp. **B.** Life cycle of *Afm*. When a conidium (C) meets proper growth conditions, it becomes a swollen conidium (isotropic growth) (SC), from which a germ tube emerges (GC, germinating conidium). Then, hyphae (filaments) develop and branch to form a dense network (mycelium). After competence is reached, some cells develop a stalk (S) on which a terminal vacuole (V) forms, where phialides (P) divide into asexual spores (conidia) that remain bound as chains. This constitute the conidiophores (CP). **C.** Morphology of an *Afm* colony. When conidia are point-inoculated on plates, hyphae grow outwards from this area and form a round-shape mycelium. Older mycelium is therefore located inward, where conidiation first occurs. The newest areas of growing mycelia form a white ringed-margin. The fraction of conidiating area is defined as the area covered by conidia (green, $\pi\times(d_C/2)^2$) divided by the area covered up to white margins ($\pi\times(d_W/2)^2$), which simplifies into $(d_C/d_W)^2$. **D.** Mophology of colonies of the indicated *Afm* strains on minimal medium (MM) supplemented with 2 % (w/v) Glc or 2 % (w/v) Xyl (first 3 rows, triplicate). The next rows present observations of these colonies under a magnifier (duplicate). Some were presented in Fig. 1C. The Δ*erdS*::P_{Xyl}-*erdS* and WT::P_{Xyl}-*erdS* strains present a strong fluffy phenotype under repressing (Glc) conditions, which is reduced under inducing conditions (Xyl). **E.** Observation (magnifier) of lawns of the indicated *Afm* strains on MM+2% Glc or MM+2% Xyl media. A high density of conidiophores is visible for the WT and Δ*erdS* strains, whereas less conidiophores are observed for the Δ*erdS*::P_{Xyl}-*erdS* and WT::P_{Xyl}-*erdS* strains, where they are embedded into aerial hyphae. **F.** Verification of *erdS* and *erdH* deletions in *Mor*. Two distinct diagnostic PCRs were conducted per locus to confirm proper CrispR mediated *erdS* and *erdH* deletions. External primers annealing upstream and downstream of the targeted loci were used to identify clones in which the targeted loci was modified as attested by band shifts. A second PCR was performed, using primers annealing into the targeted ORF, in order to attest the absence of the ORF in the genome. Numbers above the gels indicate clone identifiers. No DNA indicate control PCRs carried without any DNA. Expected sizes for each PCR and primers are indicated on the schematics. BAR indicates the resistance cassette conferring resistance to glufosinate ammonium.

Supplemental Fig. S2| A. Conidia phagocytosis assays. Adhesion on and internalization by macrophages of conidia of the indicated strains were evaluated using FITC- (green fluorescence of internalized conidia) or calcofluor white- (extracellular conidia) stained dormant and swollen conidia after 3 and 4 h of incubation.
B. *First row.* Refractive index (RI) images of WT Ku80 spores incubated for 24 hours at a multiplicity of infection (MOI) of 10 (corresponding to 70,000 macrophages and 700,000 spores). The first image was acquired at the beginning of the time-lapse. The second image corresponds to the time when the first signs of germination appear. The third image shows a later stage, where germinated spores are clearly visible. *Second row.* Refractive index (RI) images of Δ*erdS* spores incubated for 24 hours at a multiplicity of infection (MOI) of 10

(corresponding to 80,000 macrophages and 800,000 spores). The first image was acquired at the beginning of the time-lapse. The second image corresponds to the time when the first signs of germination appear. The third image shows a later stage, where germinated spores are clearly visible. *Lower table*: These *p*-values were obtained by comparing the distributions of per-spore germination times pairwise for all conditions with log-rank tests, a non-parametric method used in survival analysis to compare time-to-event datasets. This test evaluates whether the differences observed between Kaplan–Meier survival curves are statistically significant, considering both germinated and non-germinated spores. The total number of spores for each dataset was manually counted prior to germination, based on the observation that spores remain relatively immobile during the early stages of germination. Mutant spores showed delayed germination, with significant differences compared to WT (e.g., Δ*erdS*CI.7 mutant with MOI 10 *vs* WTku80 with MOI 5, p=1.45e-18). The WT with MOI 5 and 10 showed no significant difference (p=0.32), suggesting similar germination dynamics under these WT conditions. However, mutant spores with MOI 5 and 10 showed significant differences (p=2.66e-7), so the MOI had an influence on the germination in this case. These results validate the biological trends observed in the Kaplan–Meier curves and support the impact of strain and multiplicity of infection (MOI) on germination behavior. **C.** TLCs of total lipids extracted from mycelia (left TLC) or conidia (right TLC, "dormant spores", two replicates, Rep1 and Rep2) of the indicated strains. PE: phosphatidylethanolamine, PC: phosphatidylcholine, PG: phosphatidylglycerol. Erg-Asp bands are indicated by an asterisk (*). **D.** Conidia production of WT Ku80 (brown bars) or Δ*erdS* (orange bars) *Afm* strains in MM or in MM supplemented with 0.6 M NaCl or KCl to induce osmotic stress. **E.** TLC of total lipids extracted from WT *Afm* (Ku80) or Δ*erdS* mycelia grown in the presence of ammonia (10 mM, +N) or in the absence of a nitrogen source (-N). Bars quantify the Erg-Asp/PE ratio. **F.** Colony expansion rates (~growth rate) of the indicated *Afm* strains grown on agar plates containing the indicated media. Malt: malt agar plates, YG: yeast extract+1 % glucose plates, MM: minimal medium with the indicated nitrogen sources. Gln: L-glutamine, Glu: L-glutamate, Asn: L-asparagine, Asp: L-aspartate, Pro: L-proline, Ser: L-serine. **G.** Colony expansion rates (~growth rate) of the indicated *Afm* strains grown on agar plates containing MM + 2 % Glc or MM + 2 % Xyl and decreasing ammonia concentrations (10, 1 and 0 mM).

Supplemental Fig. S3| Cryo-EM workflow and analysis of the ErdS tetramer. A. Flow chart outlining cryo-EM image acquisition and processing performed to obtain a structure of ErdS tetramer. A representative micrograph and 2D class averages are shown. All processing was performed using Relion 3.1 (see Methods for details). **B.** Fourier shell correlation (FSC) curve of the final map of ErdS tetramer. The horizontal dashed line represents the criterion of FSC = 0.143. **C.** Local resolution map of ErdS tetramer. **D.** Cryo-EM density map of the ErdS tetramer. **E.** Overall structure of the ErdS tetramer.

Supplemental Fig. S4| Comparison of ErdS and FemX or LysPGS substrate-binding pockets. A. Structural comparision between ATT domains of *Afm* ErdS (orange) and *Weissella viridescens* FemX (light grey) complexed to its substrates. ErdS ergosterol-binding pocket of the GNAT II ATT domain was superimposed with FemX GNAT II domain bound to a tRNA CCA analog (PDB:4ii9). **B.** Cross-section of the ATT domain of ErdS, highlighting a composite pocket comprising the upper tRNA-binding site and the central ergosterol-binding tunnel. The protein is shown as a van der Waals surface, colored according to electrostatic potential ranging from −20 (red) to +20 (blue) kBT/e. **C-E.** Cross-sectional views of *Wvi* FemX bound to a peptidoglycan precursor (C), *Afm* ErdS with ergosterol placed

by SwissDock simulation (D), and *B. licheniformis* LysPGS (PDB: 4V36) containing L-lysine amide (LYN) and modeled peptidoglycan (PG) placed by SwissDock simulation (E). **F.** Structural comparision between ATT domains of *Afm* ErdS (orange) and *Wvi* FemX (grey).

Supplemental Fig. S5| Sequence logo of the ErdS region in which mutations were introduced. The logo was generated from a multiple alignment of 98 ErdS sequences selected across Dikarya. GNAT I residues are indicated by a grey band above the logo, the a(+) helix with a purple band, and the GNAT II region with an orange band. Residues that were mutated in *Afm* ErdS are indicated in squares. The color code is as follows. Blue: no or light effects of mutations on Erg-Asp synthesis activity, yellow: moderate effect, orange: medium effect, red: strong effect, grey: no more activity.

Supplemental Fig. S6| The sterol pocket. A. Docking shows that the sterol binding pocket of ErdS can accommodate Erg as well as Cho and diosgenin, suggesting a certain degree of plasticity. **B.** *In vitro* sterol aminoacylation by *Afm* ErdS in the presence of L-Asp, ATP, $tRNA^{Asp}$ and various sterols: TLC separation of reaction products show that ErdS aspartylates a variety of sterols regardless of the alkylyl side chain, but not lanosterol (with a methylated A-ring) or epicoprostanol (3-OH position in the α configuration). **C.** Structure of some sterols used in **B** (see also Fig. 3 for the remaining sterols). "*n*=" indicates the number of replicates made for the indicated sterols. **D.** *Afm* ErdS was expressed in *Sce* strains mutated in the Erg biosynthetic pathway (depicted in **E**). Total lipids were extracted an analyzed by TLC. ErdS expression was evaluated by Western Blot. Sterols stained with various colors depending on the mutant strain, indicating that the steryl-aspartates detected contained sterol derivatives different from Erg. **E.** Erg biosynthesis pathway in *Sce*. Enzymes indicated in yellow are those whose genes were deleted. This panel also indicates the structure of sterols intermediates. **F.** Substrates binding (Erg and CCA) in the ErdS ATT domain. **G.** Close up view of the contact between the ATT domain of ErdS (light orange), ergosterol and CCA analog. The structure of FemX (grey) is superimposed.

Supplemental Fig. S7| Growth of *Sce* Δ*dps1* strains complemented with ErdS variants (drop tests). *Sce* AspRS is represented in dark blue. For ErdS, the NTD is represented by a black line, the tRNA-binding motif in red, the AspRS domain in light blue, the ATT domain in orange. Growth of *Sce dps1*Δ complemented by either Afm or Aor ErdS is strongly reduced compared to that of *Sce dps1*Δ complemented by the *dps1* (*Sce* AspRS) gene or by ErdS ΔATT. Progressive truncation of *Afm* ErdS' NTD (ΔN30, ΔN60, ΔN84) restores growth, indicating that this domain also contributes to Asp-$tRNA^{Asp}$ utilization for Erg-Asp production over protein synthesis.

Supplemental Fig. S8| Cryo-EM workflow and analysis of the ErdS/$tRNA^{Asp}$ dimer. A-C. Flow chart outlining cryo-EM image acquisition and processing performed to obtain a structure of ErdS/tRNA dimer focusing on (B) N-terminal domain (C) and AAT domai. A representative micrograph and 2D class averages are shown. Processing was performed using Relion 3.1 and cryoSPARC v4.6.0 (see Methods for details). **D. and E.** Fourier shell correlation (FSC) curve of the final map of ErdS dimer. The horizontal dashed line represents the criterion of FSC = 0.143.

Supplemental Fig. S9| Structure of the ErdS/$tRNA^{Asp}$ dimer. A. Overall structure of the ErdS/$tRNA^{Asp}$ dimer. **B.** Cryo-EM density map of the ErdS/$tRNA^{Asp}$ dimer.

Supplemental Fig. S10| Cryo-EM workflow and analysis of the ErdS/tRNA^{Asp} dimer. A. Flow chart outlining cryo-EM image acquisition and processing performed to obtain a structure of ErdS/tRNA^{Asp} focusing on the position of CCA end of the tRNA^{Asp}. Processing was performed using Relion 3.1 and cryoSPARC v4.6.0 (see Methods for details). **B.** Fourier shell correlation (FSC) curve of the final map of ErdS/tRNA^{Asp}. The horizontal dashed line represents the criterion of FSC = 0.143.

Supplemental Fig. S11| tRNA translocation. A. Cryo-EM density map of the ErdS/tRNA^{Asp} dimer with AAT domains. **B.** Cryo-EM density map of the ErdS/Asp-*N*-tRNA^{Asp} on Asp-*N*-tRNA^{Asp} CCA end moved state.

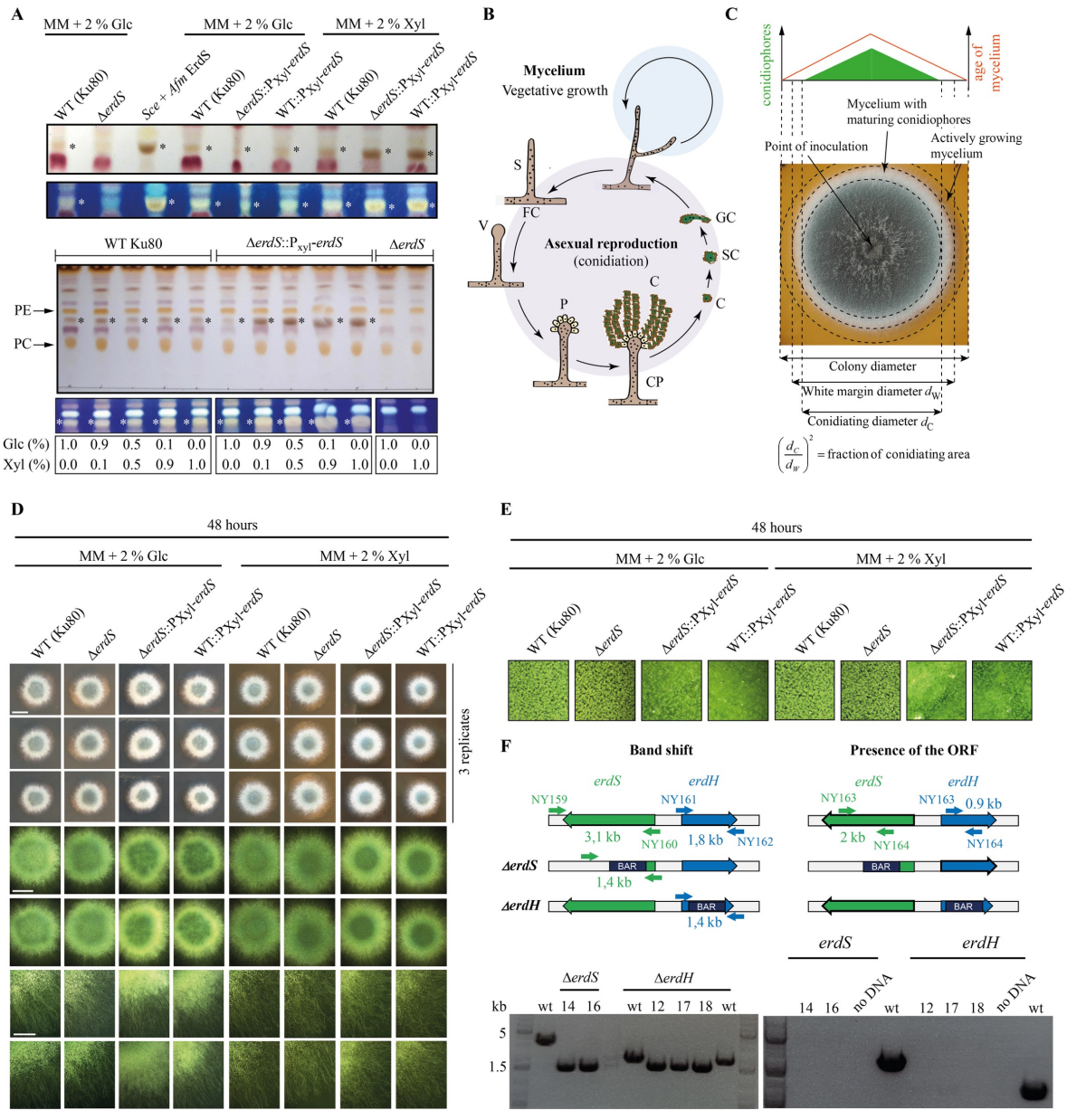
A
MM + 2 % Glc
MM + 2 % Glc
MM + 2 % Xyl
WT (Ku80)
ΔerdS
Sce + Afm ErdS
WT (Ku80)
ΔerdS::PXyl-erdS
WT::PXyl-erdS
WT (Ku80)
ΔerdS::PXyl-erdS
WT::PXyl-erdS
WT Ku80
ΔerdS::Pxyl-erdS
ΔerdS
PE
PC
Glc (%) 1.0 0.9 0.5 0.1 0.0 1.0 0.9 0.5 0.1 0.0 1.0 0.0
Xyl (%) 0.0 0.1 0.5 0.9 1.0 0.0 0.1 0.5 0.9 1.0 0.0 1.0
B
Mycelium
Vegetative growth
S
FC
V
Asexual reproduction
(conidiation)
GC
SC
C
C
P
CP
C
conidiophores
age of mycelium
Mycelium with maturing conidiophores
Point of inoculation
Actively growing mycelium
Colony diameter
White margin diameter d_W
Conidiating diameter d_C
$\left(\frac{d_C}{d_W}\right)^2$ = fraction of conidiating area
D
48 hours
MM + 2 % Glc
MM + 2 % Xyl
WT (Ku80)
ΔerdS
ΔerdS::PXyl-erdS
WT::PXyl-erdS
WT (Ku80)
ΔerdS
ΔerdS::PXyl-erdS
WT::PXyl-erdS
3 replicates
E
48 hours
MM + 2 % Glc
MM + 2 % Xyl
WT (Ku80)
ΔerdS
ΔerdS::PXyl-erdS
WT::PXyl-erdS
WT (Ku80)
ΔerdS
ΔerdS::PXyl-erdS
WT::PXyl-erdS
F
Band shift
Presence of the ORF
erdS
erdH
NY159
NY161
3,1 kb
NY160
1,8 kb
NY162
ΔerdS
BAR
1,4 kb
ΔerdH
BAR
1,4 kb
NY163
NY163
0.9 kb
2 kb
NY164
NY164
BAR
BAR
erdS
erdH
ΔerdS
ΔerdH
kb wt 14 16 wt 12 17 18 wt
5
1.5
14 16 no DNA wt 12 17 18 no DNA wt

Fig. S1

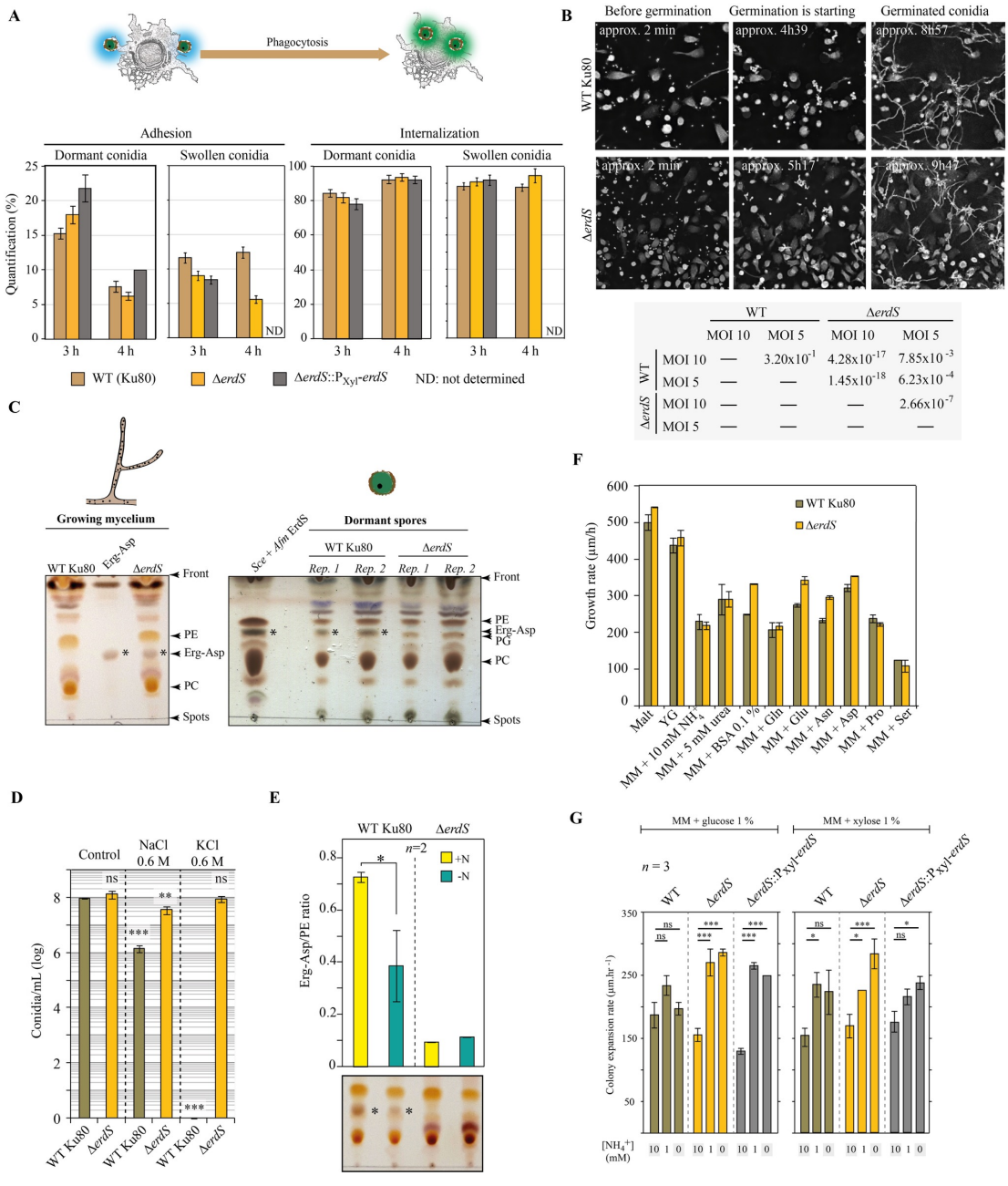
A
Phagocytosis
Adhesion
Internalization
Dormant conidia
Swollen conidia
Quantification (%)
3 h
4 h
ND
WT (Ku80)
ΔerdS
ΔerdS::PXyl-erdS
ND: not determined
B
Before germination
Germination is starting
Germinated conidia
WT Ku80
ΔerdS
approx. 2 min
approx. 4h39
approx. 8h57
approx. 5h17
approx. 9h47
WT
ΔerdS
MOI 10
MOI 5
— 3.20x10-1 4.28x10-17 7.85x10-3
— — 1.45x10-18 6.23x10-4
— — — 2.66x10-7
— — — —
C
Growing mycelium
Dormant spores
Sce + Afm ErdS
WT Ku80
ΔerdS
Erg-Asp
Rep. 1
Rep. 2
Front
PE
PG
PC
Spots
D
Control
NaCl 0.6 M
KCl 0.6 M
ns
Conidia/mL (log)
E
n=2
+N
-N
Erg-Asp/PE ratio
F
Growth rate (µm/h)
Malt
YG
MM + 10 mM NH4
MM + 5 mM urea
MM + BSA 0.1 %
MM + Gln
MM + Glu
MM + Asn
MM + Asp
MM + Pro
MM + Ser
G
MM + glucose 1 %
MM + xylose 1 %
n = 3
ΔerdS::PXyl-erdS
Colony expansion rate (µm.hr-1)
[NH4+] (mM)

Fig. S2

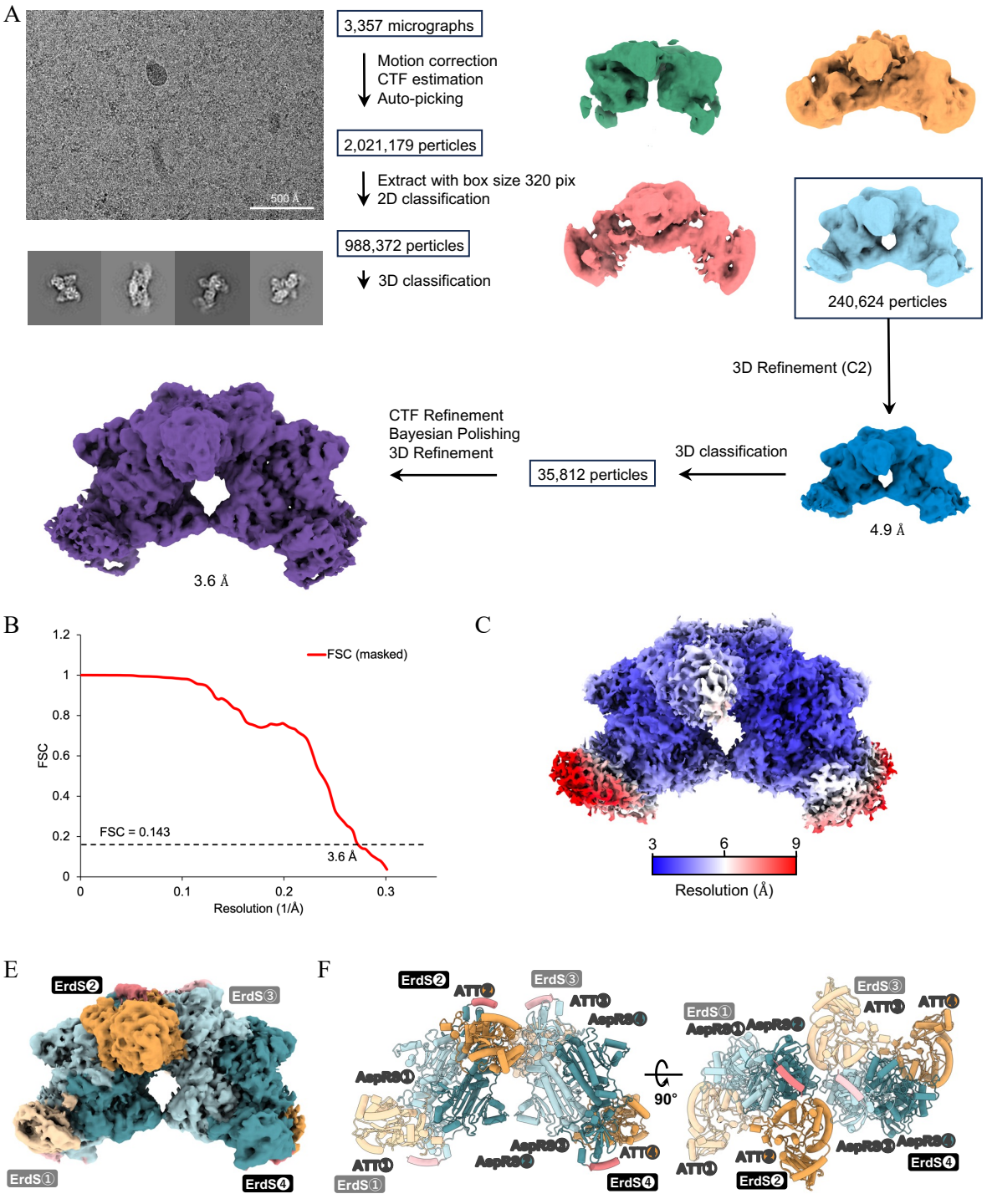
A
500 Å
3,357 micrographs
Motion correction
CTF estimation
Auto-picking
2,021,179 particles
Extract with box size 320 pix
2D classification
988,372 particles
3D classification
240,624 particles
3D Refinement (C2)
4.9 Å
3D classification
35,812 particles
CTF Refinement
Bayesian Polishing
3D Refinement
3.6 Å
B
FSC (masked)
FSC
FSC = 0.143
3.6 Å
Resolution (1/Å)
C
3
6
9
Resolution (Å)
E
ErdS②
ErdS③
ErdS①
ErdS④
F
90°

Fig. S3

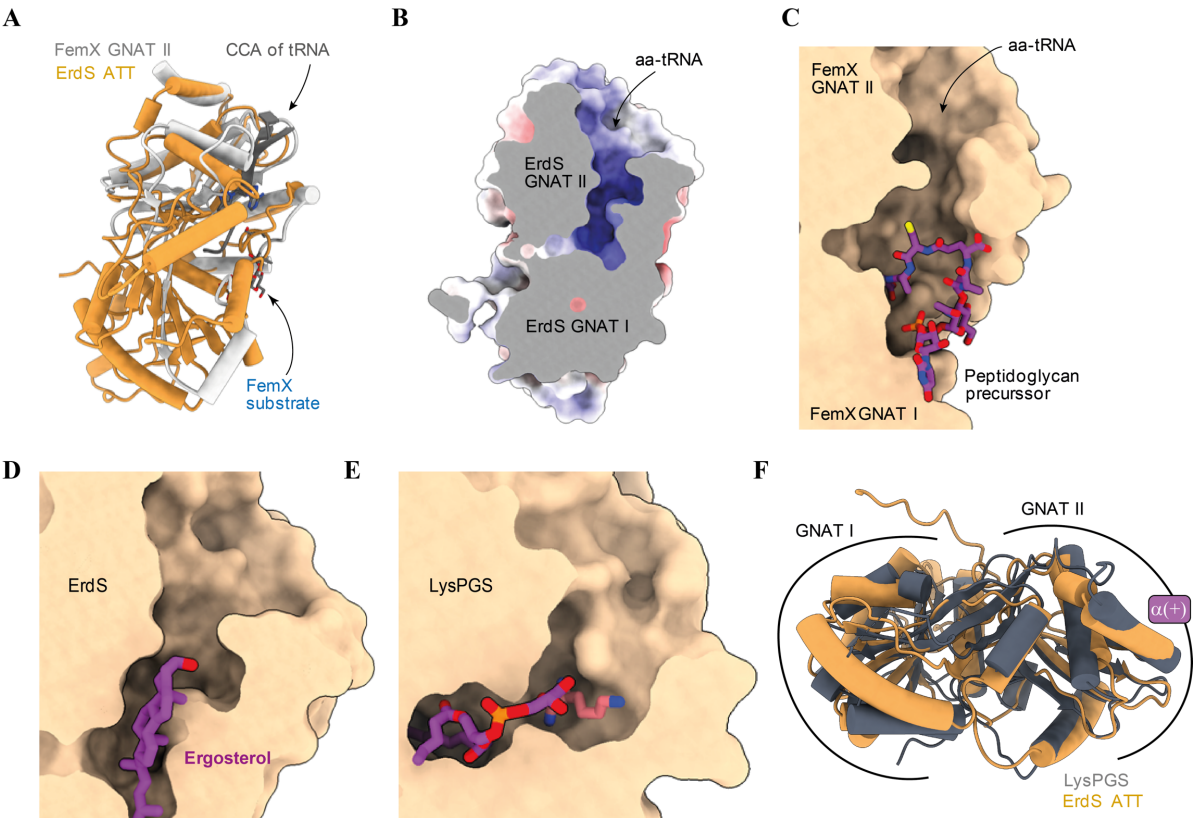
A
FemX GNAT II
ErdS ATT
CCA of tRNA
FemX
substrate
B
aa-tRNA
ErdS
GNAT II
ErdS GNAT I
C
aa-tRNA
FemX
GNAT II
Peptidoglycan
precurssor
FemX GNAT I
D
ErdS
Ergosterol
E
LysPGS
F
GNAT I
GNAT II
α(+)
LysPGS
ErdS ATT

Fig. S4

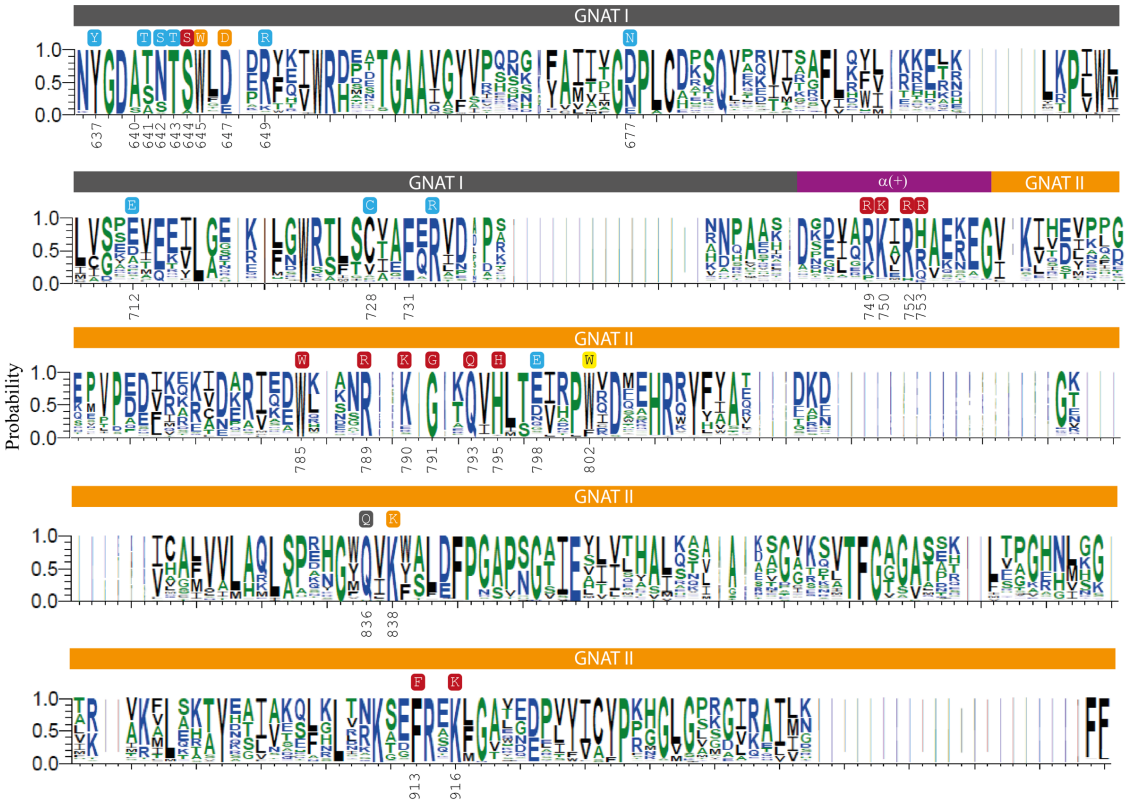
GNAT I
GNAT I
α(+)
GNAT II
GNAT II
GNAT II
GNAT II
Probability
1.0
0.5
0.0

Fig. S5

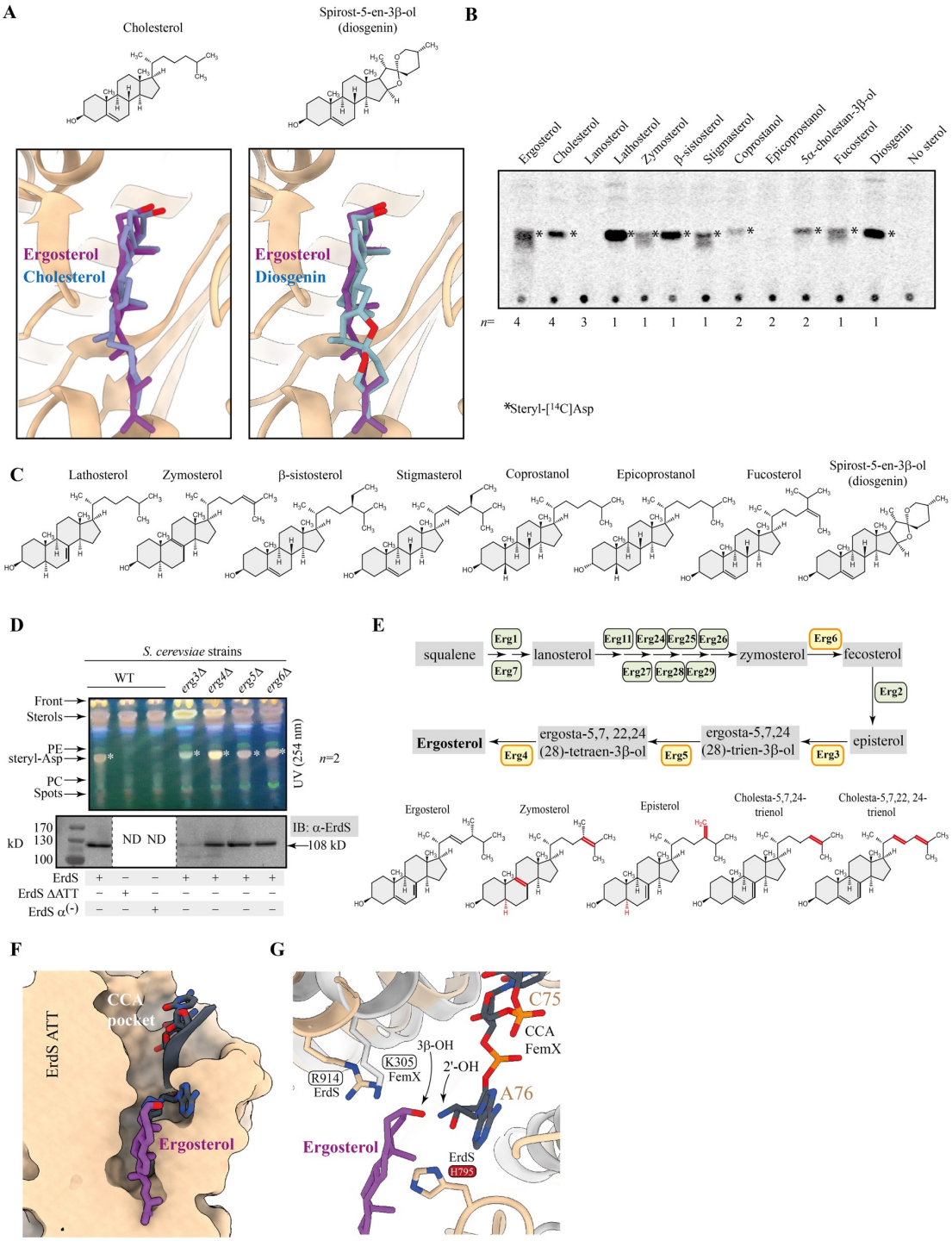
A
Cholesterol
Spirost-5-en-3β-ol (diosgenin)
Ergosterol
Cholesterol
Ergosterol
Diosgenin
B
Ergosterol
Cholesterol
Lanosterol
Lathosterol
Zymosterol
β-sistosterol
Stigmasterol
Coprostanol
Epicoprostanol
5α-cholestan-3β-ol
Fucosterol
Diosgenin
No sterol
n= 4 4 3 1 1 1 1 2 2 2 1 1
*Steryl-[14C]Asp
C
Lathosterol
Zymosterol
β-sistosterol
Stigmasterol
Coprostanol
Epicoprostanol
Fucosterol
Spirost-5-en-3β-ol (diosgenin)
D
S. cerevsiae strains
WT
erg3Δ
erg4Δ
erg5Δ
erg6Δ
Front
Sterols
PE
steryl-Asp
PC
Spots
UV (254 nm)
n=2
kD
170
130
100
ND ND
IB: α-ErdS
108 kD
ErdS
ErdS ΔATT
ErdS α(-)
E
squalene
Erg1
Erg7
lanosterol
Erg11
Erg24
Erg25
Erg26
Erg27
Erg28
Erg29
zymosterol
Erg6
fecosterol
Erg2
episterol
Erg3
ergosta-5,7,24 (28)-trien-3β-ol
Erg5
ergosta-5,7, 22,24 (28)-tetraen-3β-ol
Erg4
Ergosterol
Ergosterol
Zymosterol
Episterol
Cholesta-5,7,24-trienol
Cholesta-5,7,22, 24-trienol
F
ErdS ATT
CCA pocket
Ergosterol
G
C75
CCA
FemX
3β-OH
2'-OH
K305
FemX
R914
ErdS
A76
Ergosterol
ErdS
H795

Fig. S6

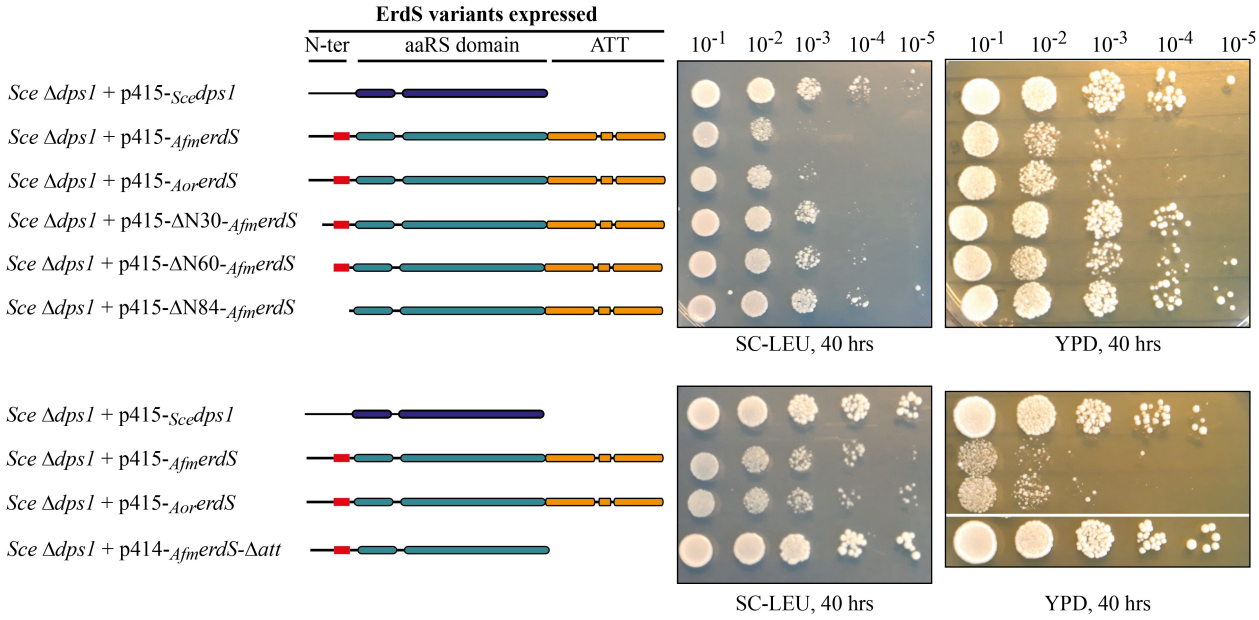
ErdS variants expressed
N-ter
aaRS domain
ATT
Sce Δdps1 + p415-Scedps1
Sce Δdps1 + p415-AfmerdS
Sce Δdps1 + p415-AorerdS
Sce Δdps1 + p415-ΔN30-AfmerdS
Sce Δdps1 + p415-ΔN60-AfmerdS
Sce Δdps1 + p415-ΔN84-AfmerdS
10-1 10-2 10-3 10-4 10-5
10-1 10-2 10-3 10-4 10-5
SC-LEU, 40 hrs
YPD, 40 hrs
Sce Δdps1 + p415-Scedps1
Sce Δdps1 + p415-AfmerdS
Sce Δdps1 + p415-AorerdS
Sce Δdps1 + p414-AfmerdS-Δatt
SC-LEU, 40 hrs
YPD, 40 hrs

Fig. S7

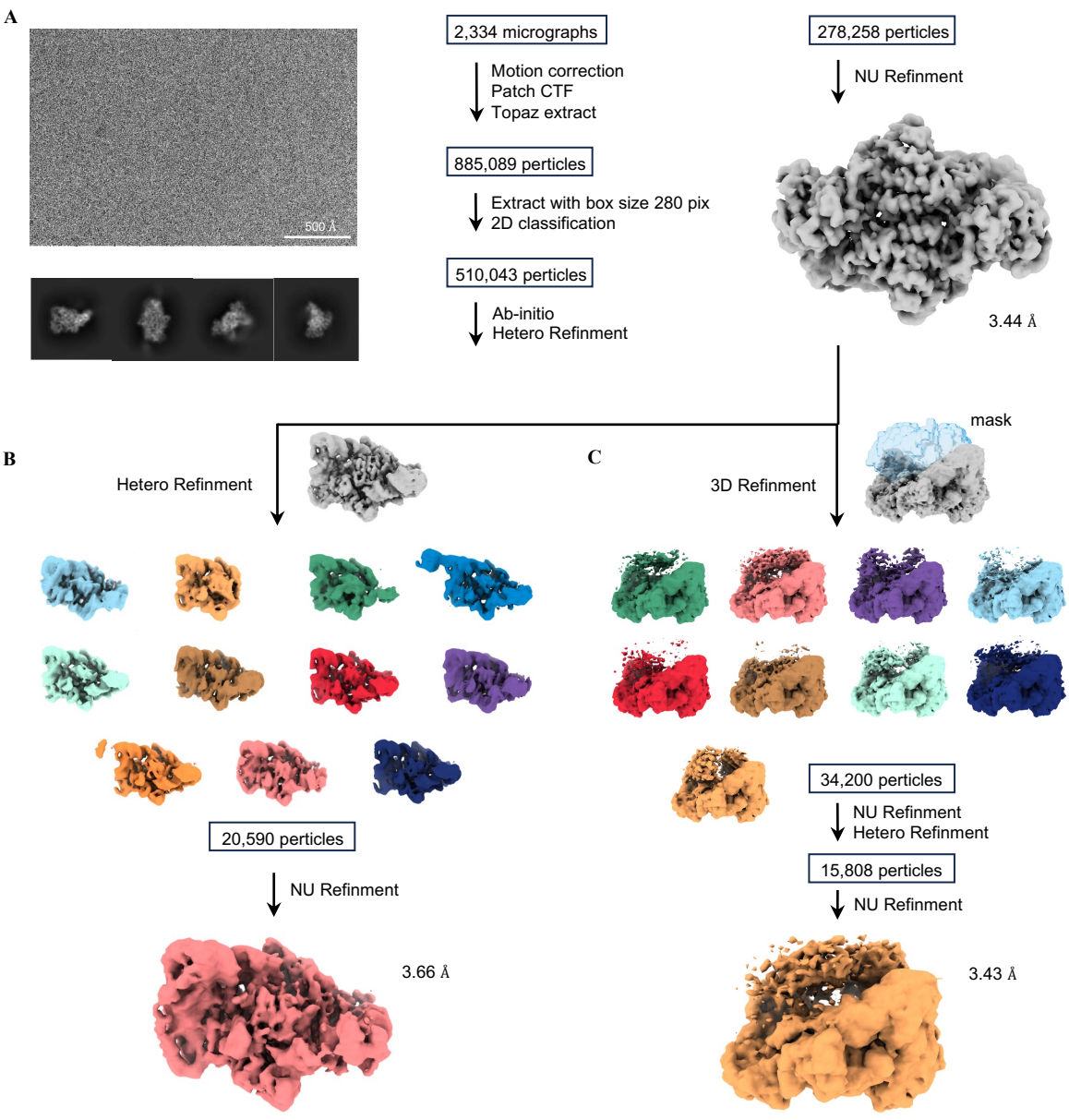
A
500 Å
2,334 micrographs
Motion correction
Patch CTF
Topaz extract
885,089 perticles
Extract with box size 280 pix
2D classification
510,043 particles
Ab-initio
Hetero Refinment
278,258 perticles
NU Refinment
3.44 Å
mask
B
Hetero Refinment
C
3D Refinment
20,590 perticles
NU Refinment
3.66 Å
34,200 perticles
NU Refinment
Hetero Refinment
15,808 perticles
NU Refinment
3.43 Å

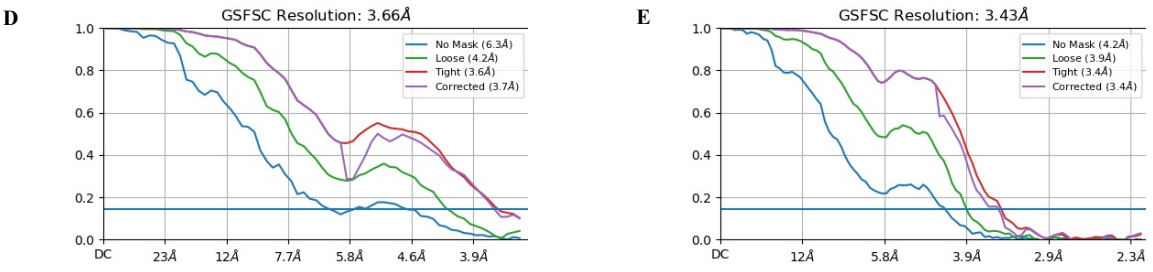
D
GSFSC Resolution: 3.66Å
No Mask (6.3Å)
Loose (4.2Å)
Tight (3.6Å)
Corrected (3.7Å)
1.0
0.8
0.6
0.4
0.2
0.0
DC
23Å
12Å
7.7Å
5.8Å
4.6Å
3.9Å
E
GSFSC Resolution: 3.43Å
No Mask (4.2Å)
Loose (3.9Å)
Tight (3.4Å)
Corrected (3.4Å)
1.0
0.8
0.6
0.4
0.2
0.0
DC
12Å
5.8Å
3.9Å
2.9Å
2.3Å

Fig. S8

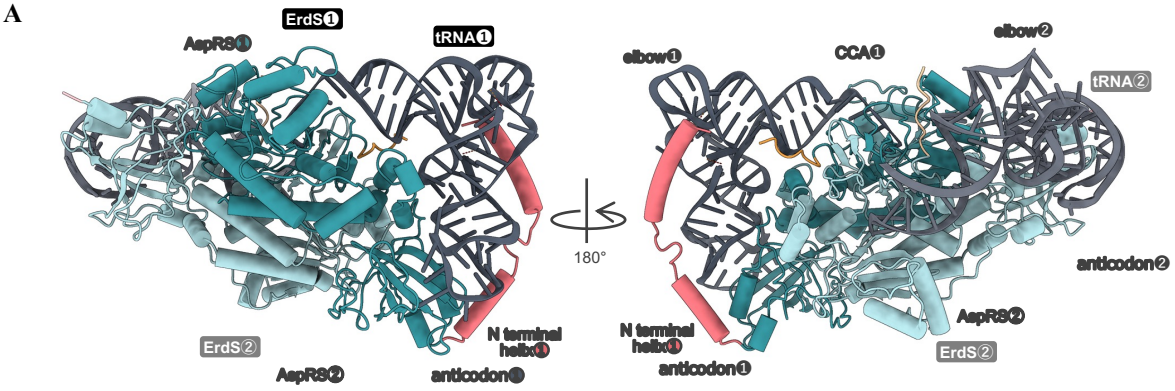
A
ErdS①
AspRS①
tRNA①
N terminal helix①
ErdS②
AspRS②
anticodon①
180°
elbow①
CCA①
elbow②
tRNA②
anticodon②
AspRS②
N terminal helix①
anticodon①
ErdS②

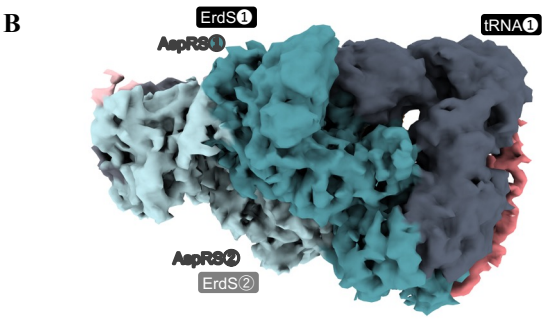
B
ErdS①
AspRS①
tRNA①
AspRS②
ErdS②

Fig. S9

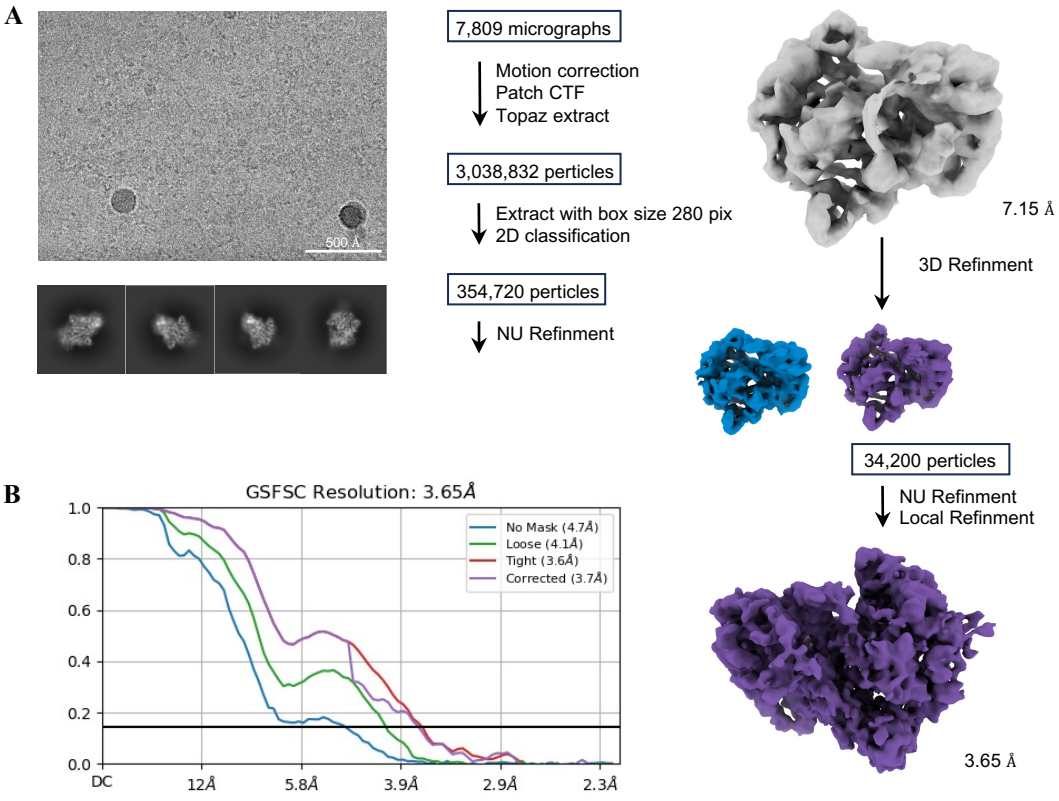
A
500 Å
7,809 micrographs
Motion correction
Patch CTF
Topaz extract
3,038,832 particles
Extract with box size 280 pix
2D classification
354,720 particles
NU Refinment
7.15 Å
3D Refinment
34,200 particles
NU Refinment
Local Refinment
3.65 Å
B
GSFSC Resolution: 3.65Å
No Mask (4.7Å)
Loose (4.1Å)
Tight (3.6Å)
Corrected (3.7Å)
1.0
0.8
0.6
0.4
0.2
0.0
DC
12Å
5.8Å
3.9Å
2.9Å
2.3Å

Fig. S10

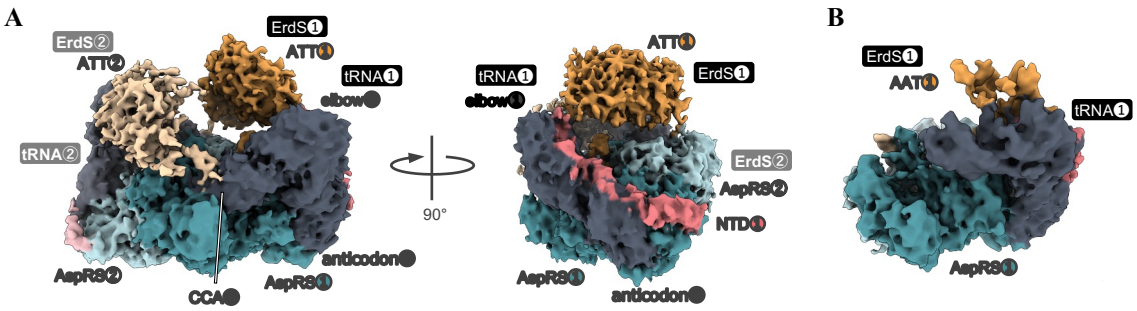
A
ErdS②
ATT②
ErdS①
ATT①
tRNA①
elbow
tRNA②
AspRS②
CCA
AspRS①
anticodon
90°
tRNA①
elbow
ATT①
ErdS①
ErdS②
AspRS②
NTD①
AspRS①
anticodon
B
ErdS①
AAT①
tRNA①
AspRS①

Fig. S11

Table S4 Refinement and model statistics

	ErdS tetramer	ErdS/tRNA dimer	
		tRNA dock	tRNA undock
PDB			-
Data collection and Processing			
Microscope	Titan Krios G3i	Titan Krios G4	Titan Krios G3i
Detector	Gatan K3 camera	Gatan K3 camera	Gatan K3 camera
Magnification	105,000	105,000	105,000
Voltage (kV)	300	300	300
Total electron exposure (e-/Å2)	49	48	51
Defocus range (um)	-0.8 to -1.6	-0.4 to -1.6	-0.4 to -1.6
Pixel size (Å)	0.83	0.83	0.83
Number of movies	3357	2334	7,809
Initial particles	326,790	894,076	3,040,852
Final particles	35,812	20,590	54,142
Symmetry imposed	C2	C1	C1
Resolution (global, Å) FSC 0.143 (masked)	3.7	3.66	3.65
Model composition			
Non-hydrogen atoms	27,724	11,571	9070
Protein residues	3,448	1,035	932
Nucleic acid residues	0	150	75
Model Refinement			
Model-Map CC (mask/volume/peaks)	0.64/0.63/0.57	0.63/0.62/0.55	0.58/0.57/0.49
Resolution (Å) by model-to map FSC, threshold 0.5 (masked/unmasked)	4.1/4.2	6.2/6.8	7.4/7.7
Average *B* factor(Å2) (Protein/Nucleotide)	128.66/-	132.27/237.80	188.13/242.73
R.M.S. deviations			
bond lengths (Å)	0.005	0.004	0.003
bond angles (°)	1.000	0.676	0.604
Validation			
MolProbity score	1.6	1.76	1.62
CaBLAM outliers (%)	1.17	1.27	1.95
Clash score	8.78	18.34	12.94
Rotamer outliers (%)	1.48	0.77	0.00
Cβ outliers (%)	0	0	0
Ramachandran plot			
Favored (%)	98.84	98.06	98.28
Allowed (%)	1.16	1.94	1.72
Outlier (%)	0.00	0.00	0.00